Supplementary materials for

Global natural wetland methane emissions (2000-2025)

Mengze Li[1,2], Robert B. Jackson[2,3], Marielle Saunois[4], Philippe Ciais[4], Ben Poulter[5], Josep G. Canadell[6], Prabir K. Patra[7,8], Hanqin Tian[9,10], Zhen Zhang[11], Etienne Fluet-Chouinard[12], Zutao Ouyang[13], Ting Zhang[1], David J. Beerling[14], Dmitry A. Belikov[15], Philippe Bousquet[4], Danilo Custodio[4], Naveen Chandra[7], Xinyu Dou[2], Nicola Gedney[16], Peter O. Hopcroft[17], Alison M. Hoyt[2], Kazuhito Ichii[15,18], Akihito Ito[19], Atul K. Jain[20], Katherine Jensen[21], Fortunat Joos[22], Thomas Kleinen[23], Masayuki Kondo[8,24], Fa Li[2], Tingting Li[25], Xiangyu Liu[26], Shamil Maksyutov[27], Avni Malhotra[28], Adrien Martinez[4], Kyle McDonald[21], Joe R. Melton[29], Paul Miller[30], Jurek Müller[22], Yosuke Niwa[27,31], Shufen Pan[9], Shushi Peng[32], Changhui Peng[33,34], Zhangcai Qin[35], Peter Raymond[36], William Riley[37], Arjo Segers[38], Rona L. Thompson[16],Aki Tsuruta[39], Xi Yi[4], Kunxiaojia Yuan[40], Wenxin Zhang[30], Bo Zheng[41,42], Qing Zhu[37], Qiuan Zhu[43], Qianlai Zhuang[26]

1 Department of Geography, National University of Singapore, Singapore.
2 Stanford Doerr School of Sustainability, Department of Earth System Science, Stanford, CA, USA.
3 Department of Earth System Science, Woods Institute for the Environment, and Precourt Institute for Energy, Stanford University, Stanford, CA, USA.
4 Laboratoire des Sciences du Climat et de l'Environnement (LSCE), CEA, CNRS, UVSQ, Université Paris Saclay, Gif-sur-Yvette, France.
5 Spark Climate Solutions, San Francisco, CA, USA.
6 Global Carbon Project, CSIRO Environment, ACT 2601, Australia.
7 Research Institute for Global Change, JAMSTEC, 3173-25 Showa-machi, Kanazawa, Yokohama, 236-0001, Japan.
8 Seto Inland Sea Carbon Neutral Research Center (S-CNC), Hiroshima University, Higashi-Hiroshima, Hiroshima 739-8529, Japan.
9 Center for Earth System Science and Global Sustainability, Schiller Institute for Integrated Science and Society, Boston College, Chestnut Hill, MA, USA.
10 Department of Earth and Environmental Sciences, Boston College, Chestnut Hill, USA.
11 State Key Laboratory of Tibetan Plateau Earth System, Environment and Resources, and Institute of Tibetan Plateau Research, Chinese Academy of Sciences, Beijing, China.
12 Earth System Science Division, Pacific Northwest National Laboratory, Richland, WA, USA.
13 College of Forestry, Wildlife and Environment, Auburn University, Auburn, AL, USA.
14 School of Biosciences, University of Sheffield, U.K.
15 Center for Environmental Remote Sensing, Chiba University, Chiba, Japan.
16 MetOffice Hadley Centre, Joint Centre for Hydrometeorological Research, Wallingford, U.K.
17 School of Geography, Earth & Environmental Sciences, University of Birmingham, U.K.
18 Graduate School of Science and Engineering, Chiba University, 1-33, Yayoi-cho, Inage-ku, Japan.
19 Graduate School of Agricultural and Life Sciences, The University of Tokyo, Tokyo, Japan.
20 Department of Climate, Meteorology, and Atmospheric Sciences, University of Illinois at Urbana-Champaign, Urbana, IL, USA.
21 Department of Earth and Atmospheric Sciences, City University of New York, New York, NY, USA.
22 Climate and Environmental Physics, Physics Institute and Oeschger Centre for Climate Change Research, University of Bern, Bern, Switzerland.
23 Max Planck Institute for Meteorology, Hamburg, Germany.

24 The IDEC Institute - Center for Peaceful and Sustainable Futures (CEPEAS), Network for Education and Research on Peace and Sustainability (NERPS), Graduate School of Humanities and Social Sciences International Economic Development Program (IEDP), Graduate School of Innovation and Practice for Smart Society (SmaSo), Hiroshima University, Higashi-Hiroshima, Hiroshima 739-8529, Japan.

25 Key Laboratory of Atmospheric Environment and Extreme Meteorology, Institute of Atmospheric Physics, Chinese Academy of Sciences, Beijing, China.

26 Department of Earth, Atmospheric, and Planetary Sciences, Department of Agronomy, Purdue University, West Lafayette, IN, USA.

27 Center for Global Environmental Research, National Institute for Environmental Studies, Tsukuba, Ibaraki, Japan.

28 Biological Sciences Division, Pacific Northwest National Laboratory, Richland, WA, USA.

29 Climate Research Division, Environment and Climate Change Canada, Victoria, BC, Canada.

30 Department of Physical Geography and Ecosystem Science, Lund University, Sölvegatan 12, 223 62, Lund, Sweden.

31 Meteorological Research Institute (MRI), Nagamine 1-1, Tsukuba, Ibaraki 305-0052, Japan.

32 Sino-French Institute for Earth System Science, College of Urban and Environmental Sciences, Peking University, Beijing 100871, China

33 Department of Biology Sciences, University of Quebec at Montreal, C.P. 8888, Succ. Centre-Ville, Montreal, QC H3C 3P8, Canada.

34 College of Geographic Science, Hunan Normal University, Changsha 410081, China.

35 School of Atmospheric Sciences, Sun Yat-sen University, and Southern Marine Science and Engineering Guangdong Laboratory (Zhuhai), Zhuhai 519000, China.

36 School of the Environment, Yale University, New Haven, CT, USA.

37 Climate and Ecosystem Sciences Division, Lawrence Berkeley National Laboratory, Berkeley, CA, USA.

38 TNO, Department of Climate Air & Sustainability, P.O. Box 80015, NL-3508-TA, Utrecht, the Netherlands.

39 Finnish Meteorological Institute, P.O. Box 503, 00101, Helsinki, Finland.

40 Department of Earth and Atmospheric Sciences, University of Houston, Houston, TX, USA.

41 Institute of Environment and Ecology, Tsinghua Shenzhen International Graduate School, Tsinghua University, Shenzhen 518055, China.

42 State Environmental Protection Key Laboratory of Sources and Control of Air Pollution Complex, Beijing 100084, China.

43 College of Hydrology and Water Resources, Hohai University, Nanjing 210098, China.

Correspondence to: Mengze Li (mengze@nus.edu.sg)

Table S1. Bottom-up (BU) models used in this study.

BU model	Wetland extent mode	Climate forcings used (each as an individual estimate)
CLASSIC	Prognostic	CRU; GSWP3-W5E5
ELM-ECA	Prognostic	CRU; GSWP3-W5E5
ISAM	Prognostic	CRU; GSWP3-W5E5
JSBACH	Prognostic	CRU; GSWP3-W5E5
JULES	Prognostic	CRU; GSWP3-W5E5
LPJ-MPI	Prognostic	CRU; GSWP3-W5E5
LPJ-WSL	Prognostic	CRU; GSWP3-W5E5
LPX-Bern	Prognostic	CRU; GSWP3-W5E5
ORCHIDEE	Prognostic	CRU; GSWP3-W5E5
SDGVM	Prognostic	CRU; GSWP3-W5E5
VISIT	Prognostic	CRU; GSWP3-W5E5

Table S2. Top-down (TD) atmospheric inversions used in this study.

Run ID	Inversion system	Observation constraint	Variant label*
1	CIF-LMDz	SURF	inv1
2	CIF-LMDz	SURF	inv2
3	CTE	SURF	inv1
4	CTE	SURF	inv2
5	MIROC4-ACTM	SURF	inv1
6	MIROC4-ACTM	SURF	inv2
7	NIES	SURF	inv1
8	NIES	SURF	inv2
9	NISMON-CH4	SURF	inv1
10	NISMON-CH4	SURF	inv2
11	PYVAR-LMDz	GOSAT	inv1
12	PYVAR-LMDz	SURF	inv2
13	NIES	GOSAT	inv1

*inv1 and inv2 are two inversion rounds differing in prior anthropogenic emission choices (EDGARD v6 vs GAINS for fossil fuel emissions) and in OH assumptions.

Table S3. XGBoost hyperparameter configurations.

Combo ID	Learning rate	Max tree depth	Min child weight	Subsample ratio	Column subsample per tree	L2 regularization
1	0.10	6	0.00	0.98	0.98	1.0
2	0.10	5	0.25	0.95	0.95	1.0
3	0.07	5	0.50	0.90	0.90	1.5
4	0.07	4	0.50	0.90	0.90	1.5
5	0.05	4	1.00	0.85	0.85	2.0
6	0.05	3	1.00	0.85	0.80	2.0

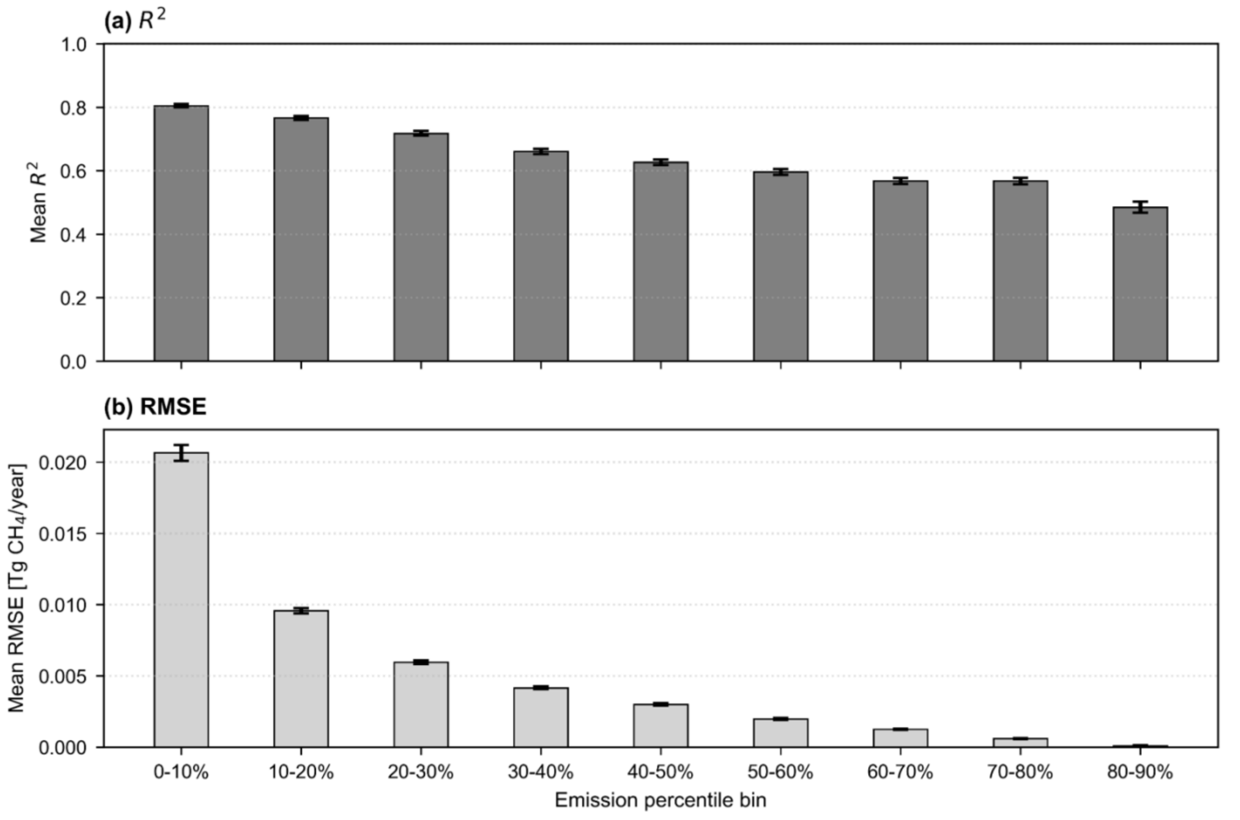

Figure S1. Reconstruction skills across regions by emission magnitude. Mean grid-cell R^2 and RMSE on the test periods, summarized within emission percentile bins defined from grid-cell wetland CH_4 emissions during 2000-2020 from GMB estimates. 0-10% denotes the highest emitting grid cells. Error bars indicate 95% CI.

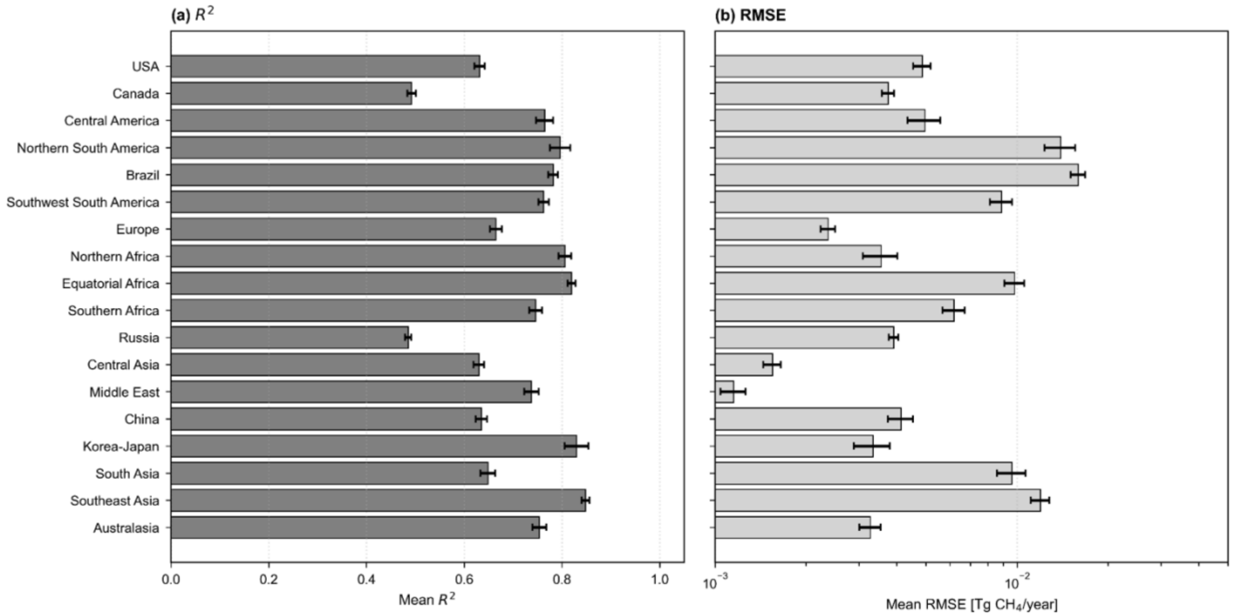

Figure S2. Reconstruction skills across 18 geographical regions. Mean grid-cell R^2 and RMSE on the test periods, summarized within emission percentile bins defined from grid-cell wetland CH_4 emissions during 2000-2020 from GMB estimates. 0-10% denotes the highest emitting grid cells. Error bars indicate 95% CI.

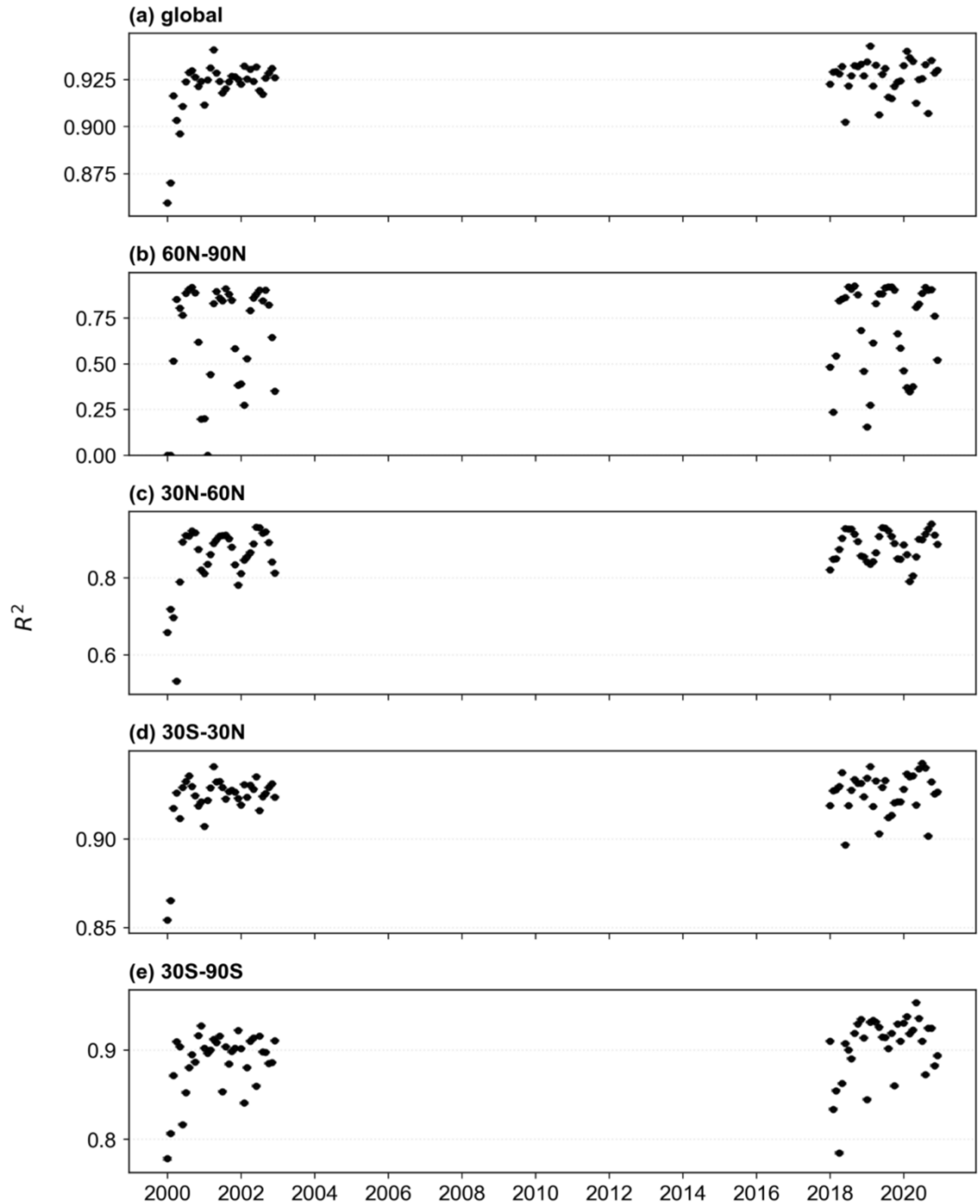

Figure S3. Mean monthly R^2 over test periods at five latitude bands. Dots and error bars indicate the mean and 95% CI.

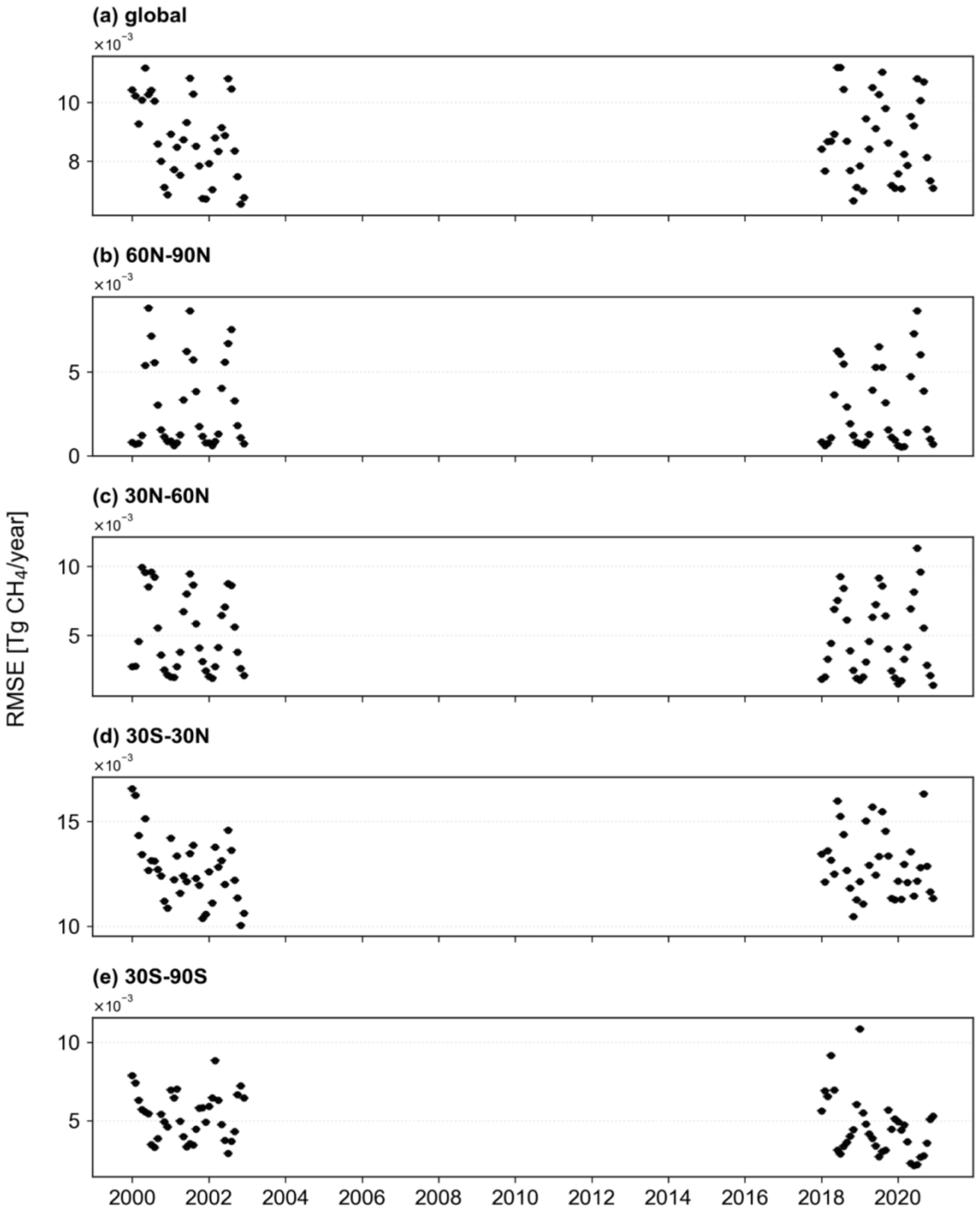

Figure S4. Mean monthly RMSE over test periods at five latitude bands. Dots and error bars indicate the mean and 95% CI.

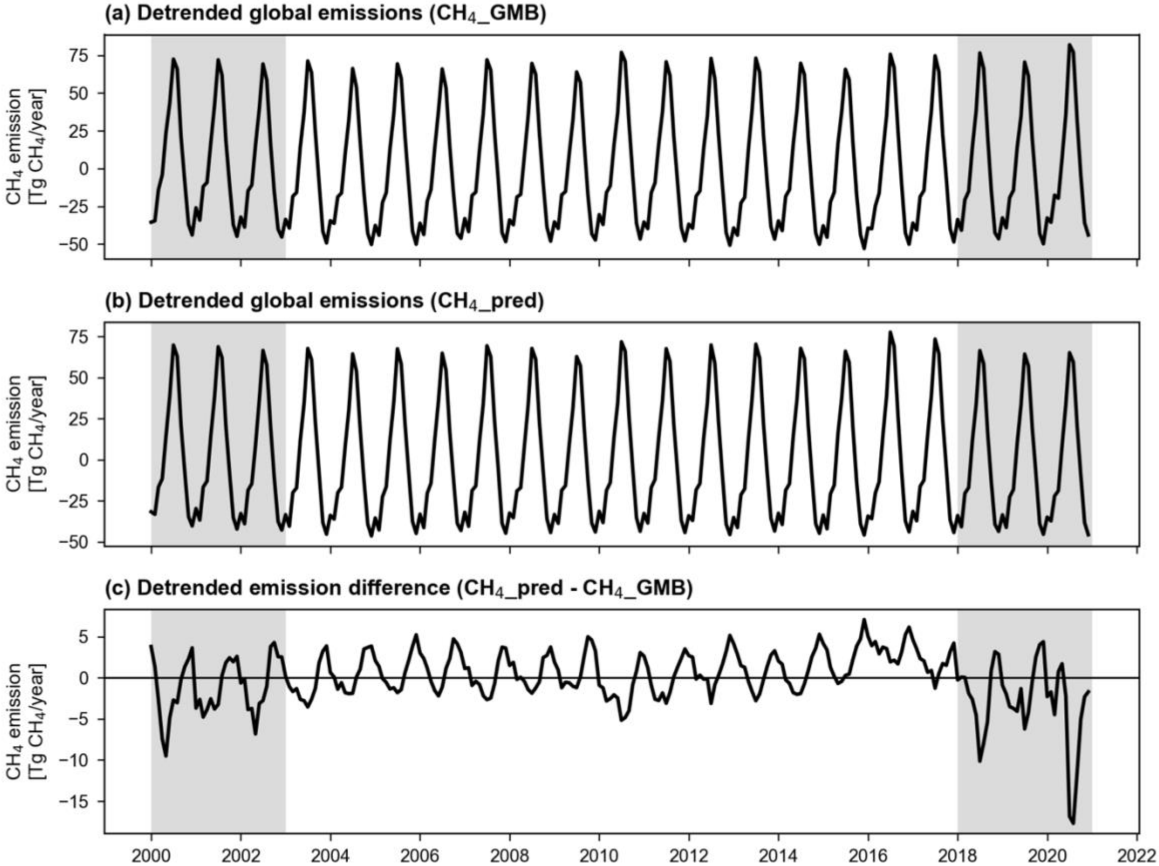

Figure S5. Detrended anomaly comparison of global wetland CH_4 emissions from GMB models (CH_4_GMB) and predictions (CH_4_pred). Detrended anomalies are calculated by removing the best-fit linear trend from each time series for the period 2000-2020. Shaded areas indicate test periods used for out-of-sample evaluation.

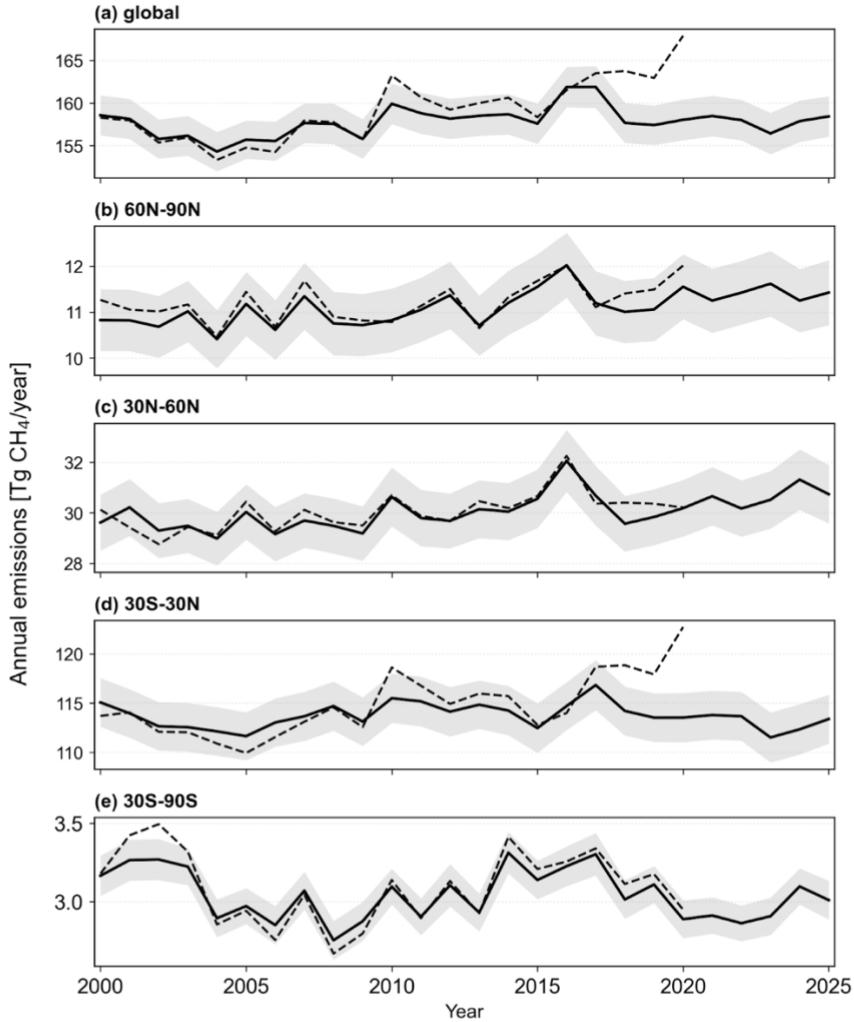

Figure S6. Annual wetland CH_4 emissions in five latitude bands. Annual mean emissions for global, 60-90°N, 30-60°N, 30°S-30°N, and 90-30°S from 2000-2025. Solid lines show model predictions of annual mean emissions and shaded areas indicate 95% CI. Dashed lines show GMB emission estimates.

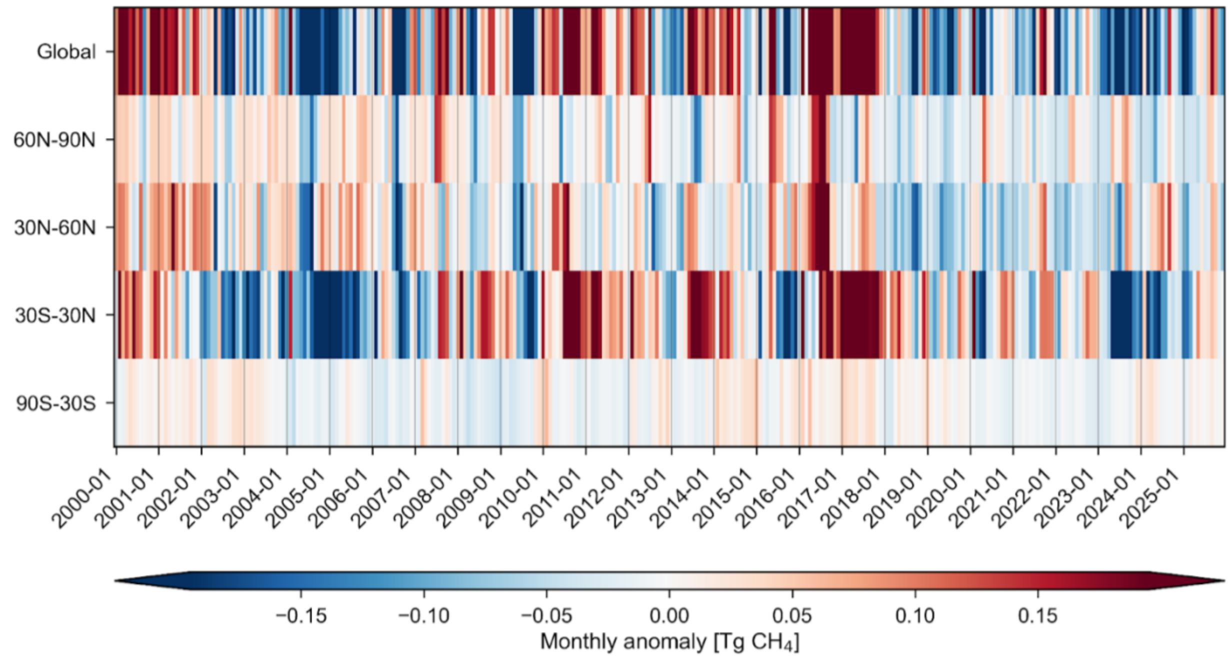

Figure S7. Monthly anomalies of wetland CH_4 emissions at five latitude bands (2000-2025). For each band, anomalies are relative to the 2000-2025 linearly detrended seasonal climatology (least squares), using predicted wetland CH_4 emissions from the XGBoost models.

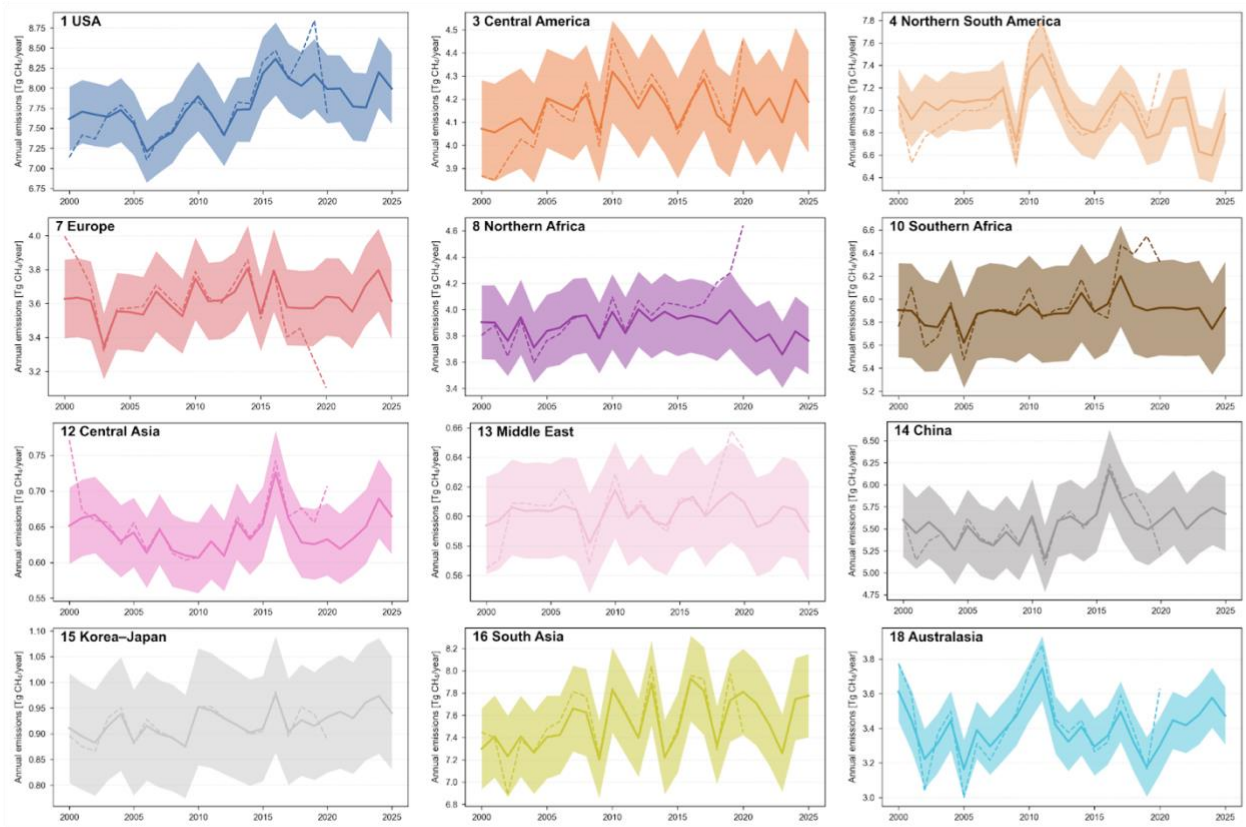

Figure S8. Annual wetland CH_4 emissions for the remaining 12 regions. Same as Figure 6, but for the other 12 regions not included in Figure 6. Solid lines show model predictions of annual mean emissions and shaded areas indicate 95% CI. Dashed lines show GMB emission estimates (mean). Panel titles indicate the region code and region name, which correspond to the region definitions shown in Figure 4.